Received: 26 June 2020 | Revised: 31 August 2020 | Accepted: 31 August 2020

DOI: 10.1002/bit.27553

ARTICLE

BIOTECHNOLOGY AND BIOENGINEERING WILEY

Recombinant protein production-associated metabolic burden reflects anabolic constraints and reveals similarities to a carbon overfeeding response

Zhaopeng Li[1] | Ursula Rinas[1,2]

[1]Leibniz University of Hannover, Technical Chemistry - Life Science, Hannover, Germany

[2]Helmholtz Centre for Infection Research, Braunschweig, Germany

Correspondence

Ursula Rinas, Helmholtz Centre for Infection Research, Inhoffenstraße 7, D-38124, Braunschweig, Germany.
Email: Ursula.Rinas@helmholtz-hzi.de

Funding information

German Ministry of Education and Research, Grant/Award Number: FKZ 0315285; German Research Council (DFG), Grant/Award Number: Rebirth EXC62

Abstract

A comparison of the metabolic response of *Escherichia coli* BL21 (DE3) towards the production of human basic fibroblast growth factor (hFGF-2) or towards carbon overfeeding revealed similarities which point to constraints in anabolic pathways. Contrary to expectations, neither energy generation (e.g., ATP) nor provision of precursor molecules for nucleotides (e.g., uracil) and amino acids (e.g., pyruvate, glutamate) limit host cell and plasmid-encoded functions. Growth inhibition is assumed to occur when hampered anabolic capacities do not match with the ongoing and overwhelming carbon catabolism. Excessive carbon uptake leads to by-product secretion, for example, pyruvate, acetate, glutamate, and energy spillage, for example, accumulation and degradation of adenine nucleotides with concomitant accumulation of extracellular hypoxanthine. The cellular response towards compromised anabolic capacities involves downregulation of cAMP formation, presumably responsible for subsequently better-controlled glucose uptake and resultant accumulation of glucose in the culture medium. Growth inhibition is neglectable under conditions of reduced carbon availability when hampered anabolic capacities also match with catabolic carbon processing. The growth inhibitory effect with accompanying energy spillage, respectively, hypoxanthine secretion and cessation of cAMP formation is not unique to the production of hFGF-2 but observed during the production of other proteins and also during overexpression of genes without transcript translation.

KEYWORDS

carbon overfeeding response, energy spilling and hypoxanthine secretion, *Escherichia coli*, recombinant protein production-associated metabolic burden

1 | INTRODUCTION

High-level recombinant protein production in *Escherichia coli* can lead to enhanced acetate secretion and growth inhibition, a phenomenon frequently described as "metabolic burden." The main reason for the protein production associated metabolic burden has been attributed to drainage of precursors and energy away from host cell maintenance and growth towards recombinant gene/plasmid related functions. Enhanced acetate formation and the resultant growth inhibition is also observed when *E. coli* is growing under nutrient excess conditions, a phenomenon generally known as "carbon overflow" metabolism. For both phenomena, energetic constraints have been held responsible, primarily the differences in proteome cost of energy biogenesis by respiration and fermentation (Basan et al., 2015; Mori, Marinari, & De, 2019; Zeng & Yang, 2019a, 2019b). In this context, overproduction of "useless" proteins has been considered to amplify the problem of carbon overflow metabolism by reducing the fraction of the host cell proteome available for energy production and biomass synthesis. These considerations imply that cells producing recombinant proteins may experience shortages in energy and biomass precursors. Protein synthesis is, compared to the synthesis of the other cellular macromolecules, a more energy-demanding process (Kaleta, Schäuble, Rinas, & Schuster, 2013; Stouthamer, 1973) in particular if energy requirements for protein folding-associated purposes have to be taken into account (Corrales & Fersht, 1996; Sharma, De los, Christen, Lustig, & Goloubinoff, 2010; Szabo et al., 1994). Moreover, recombinant-protein producing cells require (deoxy)ribonucleotides for plasmid DNA synthesis and recombinant gene transcription as well as amino acids for the production of the recombinant protein potentially leading to a shortage of these precursors for host cell proliferation.

The most common *E. coli*-based expression system is the bacteriophage T7 RNA polymerase and T7 promoter controlled gene expression combination. Isopropyl β-D-1-thiogalactopyranoside (IPTG) induction of the chromosomally encoded T7 polymerase leads to high-level expression of T7 promoter-controlled genes and correspondingly high recombinant protein titers (Studier & Moffatt, 1986). Usually, production of recombinant proteins is carried out in *E. coli* B strains which are more robust with a lower tendency to form acetate compared to *E. coli* K strains (Shiloach & Rinas, 2009; Shiloach, Kaufmann, Guillard, & Fass, 1996). Most commonly, *E. coli* BL21 (DE3) is employed as it already contains the chromosomally encoded bacteriophage T7 RNA polymerase gene. Recently, it has been shown that even recombinant gene transcription without translation leads to growth inhibition in the *E. coli* BL21 (DE3) T7-based expression system (Li & Rinas, 2020; Mittal, Brindle, Stephen, Plotkin, & Kudla, 2018) challenging the hypothesis that energy constraints are the major factors leading to the metabolic burden.

In this contribution, we analyze the impact of T7-promoter-controlled recombinant protein production on *E. coli* BL21 (DE3) metabolism in fed-batch cultures with special emphasis on the changes in glucose uptake and by-product formation (e.g., acetate, pyruvate, and glutamate) as well as on the changes in the profiles of energy-rich nucleotides (e.g., ATP) including their degradation products and regulatory molecules such as (p)ppGpp and cAMP. Moreover, we also follow the profiles of these compounds in fed-batch cultures in the absence of induced protein production but in response to carbon overfeeding.

2 | MATERIALS AND METHODS

2.1 | Strain and plasmids

E. coli BL21 (DE3; Novagen) harboring the plasmids pET-29c-hFGF-2 (Hoffmann, van den Heuvel, Zidek, & Rinas, 2004), pET-28c-His6-GFP (Li, Kessler, van den Heuvel, & Rinas, 2011) and pETM30-His6-GST-GFP (Li et al., 2011) were used for the production of hFGF-2, green fluorescent protein (GFP); and GST-GFP, respectively. For expression of the hFGF-2 gene without recombinant protein production, the plasmid pET-29c-hFGF-2-ΔRBS with the intact promoter region and ribosome binding site deletions were used (Li & Rinas, 2020). The expression vector pET-28c without any inset was from Novagen.

2.2 | Medium and cultivation conditions

The composition of Luria-Bertani (LB) broth was as follows: 10 g L^{-1} tryptone, 5 g L^{-1} yeast extract, and 5 g L^{-1} NaCl. The pH was adjusted to pH 7 with NaOH before autoclaving. For solidification, 15 g L^{-1} agar was added. The composition of the defined glucose-supplemented mineral salt media for batch (shake flask and bioreactor) and fed-batch bioreactor cultures were essentially as described previously (Korz, Rinas, Hellmuth, Sanders, & Deckwer, 1995) with slight modifications. The composition of the batch medium for bioreactor cultures was as follows: 1.65 g L^{-1} glucose·H_2O, 1.2 g L^{-1} $MgSO_4 \cdot 7H_2O$, 2.5 g L^{-1} $(NH_4)_2HPO_4$, 13.3 g L^{-1} KH_2PO_4, 1.86 g L^{-1} citric acid·H_2O, 100.8 mg L^{-1} Fe(III) citrate, 2.1 mg L^{-1} $Na_2MoO_4 \cdot 2H_2O$, 2.5 mg L^{-1} $CoCl_2 \cdot 6H_2O$, 15 mg L^{-1} $MnCl_2 \cdot 4H_2O$, 1.2 mg L^{-1} $CuCl_2$, 3 mg L^{-1} H_3BO_3, 33.8 mg L^{-1} $Zn(CH_3COOH)_2 \cdot 2H_2O$, 18 mg L^{-1} Na_2-EDTA·$2H_2O$. TEGO® Antifoam 204 (0.2 g L^{-1}; Evonik) was added to the batch medium for the bioreactor cultivation. Glucose·H_2O (12 g L^{-1}) was used for the defined non-inducing broth (DNB) in shake-flask precultures. The pH was adjusted to pH 6.8 using NaOH before autoclaving. The composition of the feeding solution was as follows: 110 g L^{-1} glucose·H_2O, 7.55 g L^{-1} $MgSO_4 \cdot 7H_2O$, 40 mg L^{-1} Fe(III) citrate, 4 mg L^{-1} $Na_2MoO_4 \cdot 2H_2O$, 4 mg L^{-1} $CoCl_2 \cdot 6H_2O$, 23.5 mg L^{-1} $MnCl_2 \cdot 4H_2O$, 1.81 mg L^{-1} $CuCl_2$, 4.7 mg L^{-1} H_3BO_3, 16 mg L^{-1} $Zn(CH_3COOH)_2 \cdot 2H_2O$, 16.55 mg L^{-1} Na_2-EDTA·$2H_2O$. Glucose·H_2O (330 g L^{-1}) was used in the feeding solution for the carbon overfeeding experiment. The feeding solution was sterilized by filtration through a 0.22 μm filter. Details of medium preparation are given elsewhere (Li, Nimtz, & Rinas, 2014). For plasmid maintenance, 50 mg L^{-1} kanamycin was added to the medium.

Precultures were prepared as follows: glycerol stocks of recombinant *E. coli* were streaked on LB agar plates and incubated overnight at 37°C. A single colony from an LB agar plate was transferred to LB medium. The cultures were shaken at 30°C for 6 h to inoculate the DNB overnight pre-culture at 30°C with a starting OD_{600} of 0.005. Shake flask cultivations were carried out using 100 or 500 ml Erlenmeyer flasks containing 10 or 50 ml medium, respectively, at 30°C and 250 rpm using a shaker with an amplitude of 5 cm. DNB pre-cultures were used to inoculate the bioreactor main cultures with a starting OD_{600} of 0.2. Bioreactor cultivations were carried out in a 2 L stainless steel bioreactor (B. Braun Biotech International) containing 1.5 L initial batch medium. During bioreactor cultivations, temperature and aeration were set at 30°C and 1 vvm, respectively. Dissolved oxygen (DO) was automatically controlled at a level greater than 40% by changing agitation speed (300–1100 rpm). For the maintenance of the DO level in the carbon overfeeding experiment, the inlet air was slowly enriched with pure oxygen after the agitation speed reached the maximum. The pH was automatically controlled at pH 6.8 by the addition of ammonia solution (25%). After consumption of the initial glucose indicated by an increase of the dissolved oxygen concentration, the fed-batch phase was started using an exponentially increasing feeding rate. Feeding was carried out essentially as described previously (Korz et al., 1995) to maintain a predetermined specific growth rate of 0.35 h^{-1} (μ_{set} = 0.35 h^{-1}). When the optical density reachedOD_{600} of 10, the cultivations were either induced by the addition of 1 mM IPTG or for the carbon overfeeding experiment, the predetermined specific growth rate was increased from 0.35 h^{-1} (μ_{set} = 0.35 h^{-1}) to 0.70 h^{-1} (μ_{set} = 0.70 h^{-1}). For reduced carbon feeding, the predetermined specific growth rate was set to μ_{set} = 0.12 h^{-1} during the entire fed-batch phase of the cultivation.

2.3 | Sampling procedure

To minimize the time between sampling from the bioreactor and the inactivation of metabolic activities, a self-made fast sampling port was installed at the side of the bioreactor. The cultivation broth and outside environment were separated by a bromobutyl rubber septum (Sartorius Stedim Biotech) and a 2 mm silicone membrane (thickness, 2 mm). For the analysis of intracellular metabolites (ATP, ADP, AMP, cAMP, GTP, and (p)ppGpp), a perchloric acid (PCA) extraction method was utilized to ensure immediate cell lysis and quenching of all metabolic activities. A pre-weighted 2 ml disposable syringe was filled with approx. 0.6 g 35% PCA (wt/wt, about 5.8 M) containing 80 mM Na_2-EDTA as described previously (Cserjan-Puschmann, Kramer, Duerrschmid, Striedner, & Bayer, 1999). To prevent precipitation of Na_2-EDTA in 35% PCA, this acidic solution was kept at 37°C. Through the self-made fast sampling port, about 1 ml sample was quickly taken from the bioreactor by a hypodermic needle (Φ0.8 × 120 mm; B. Braun Melsungen AG) to the pre-weighted 2 ml disposable syringe containing 35% PCA and 80 mM Na_2-EDTA. The acidified sample was vortexed for 10 min for complete cell disruption. After vortexing, the sample was transferred to a pre-weighed 15 ml conical centrifuge tube. The sample was neutralized to about pH 7.4 by a base (4 M KOH, 2% formaldehyde) in an ice bath. The cell debris and insoluble $KClO_4$ were removed by centrifugation at 17,000*g* and 3°C for 5 min. Finally, the supernatant was aliquoted into 1.5 ml centrifuge tubes, frozen in liquid nitrogen, and stored at −80°C. Analysis of high energy compounds (e.g., ATP and GTP) was performed as quickly as possible after the end of the cultivation. For the determination of the sample volume, at each step, the weight of the sample together with the syringe or centrifuge tube was measured assuming a sample density of 1.016 g ml^{-1}. For the determination of glucose and extracellular metabolites (acetate, pyruvate, glutamate, uracil, hypoxanthine, and extracellular cAMP), about 1 ml sample was taken from the bioreactor employing the same method as described above using an empty 2 ml disposable syringe. The cultivation broth was immediately centrifuged at 17,000*g* and 3°C for 3 min. The supernatant was filtrated through a 0.2 μm membrane, aliquoted to 1.5 ml centrifuge tubes, and stored at −80°C. The cell pellet was also stored at −80°C.

2.4 | HPLC analysis

Glucose, acetate, and pyruvate were quantified using a high-performance liquid chromatography system (HPLC; Hitachi) with a built-in diode-array detector (DAD) and an L-7490 refractive index (RI) detector (Merck) using an Aminex HPX-87H column (Bio-Rad) with a Carbo-H SecurityGuard™ cartridge (4 mm x 3.0 mm; Phenomenex). Agilent OpenLAB CDS Software (Agilent) was employed for system control and data acquisition. Before HPLC injection, all samples were filtered through a 0.2-μm syringe filter, and a 20 μl culture supernatant were used for injection (Millex GV; Millipore). Operating conditions were as follows: temperature 60°C, flow rate of 0.6 ml min^{-1}, isocratic mobile phase 20 mM H_2SO_4. The DAD at absorbance 254 nm was employed for the detection of pyruvate and the L-7490 RI detector for glucose and acetate.

Glutamate was quantified using an HPLC system (Hitachi) with an ALIAS™ autosampler (Spark Holland), an RF-20A fluorescence detector (Shimadzu) and a 3.5 μm Zorbax Eclipse Plus C18 column (4.6 mm × 150 mm; Agilent) connected with a C-18 Supelguard Cartridge (4 mm × 3.0 mm; Phenomenex). Clarity VA Chromatography Software (DataApex) was used for system control and data acquisition. Culture supernatants (50 μl) were mixed with 200 μl ice-cold methanol (−20°C) and stored overnight at −20°C. Precipitates were removed by centrifugation at 17,000*g* and 3°C for 20 min. The supernatant (50 μl) was alkalized by the addition of 50 μl cold sodium borate buffer (400 mM H_3BO_3, pH 10 by NaOH at 4°C). OPA/FMOC derivatization of amino acids in this solution (15 μl) was carried out in the ALIAS autosampler. To each vial containing a 15 μl sample, 20 μl OPA reagent (100 mg *o*-phthalaldehyde and 65 μl 3-mercaptopropionic acid dissolved in 5 ml methanol and 5 ml sodium borate buffer, 400 mM H_3BO_3, pH 10 by NaOH) were added and mixed. Following this, 15 μl FMOC reagent (9 mg 9-fluorenylmethoxycarbonyl chloride dissolved in

10 ml acetonitrile) was added and mixed. Lastly, 25 µl injection diluent (10 ml of buffer A [40 mM NaH_2PO_4, pH 7.8, 5 mM NaN_3] supplemented with 40 µl concentrated H_3PO_4) were added and mixed. From this OPA/FMOC-derivatized sample mixture 15 µl were used for injection. The operating conditions were as follows: temperature 40°C and a flow rate of 1.5 ml min^{-1}. The mobile phases consisted of two eluents: buffer A (40 mM NaH_2PO_4, pH 7.8, 5 mM NaN_3) and buffer B (45% methanol, 45% acetonitrile, and 10% H_2O). The following gradient was used: 4%–57% buffer B for 20 min, 100% buffer B for 3.5 min, and then equilibration at 4% buffer B for 5.5 min to restore the initial condition. RF-20A fluorescence detector (Shimadzu) was used for the detection of derivatized amino acids. The signal program was as follows: 0–17.5 min excitation at 330 nm and emission at 420 nm; the signal was zeroed at 0.01 min. Excitation from 17.5–25 min was set at 266 nm and emission at 305 nm; the signal was re-zeroed at 18 min.

Quantitative analyses of nucleotides and nucleobases (cAMP, ATP, ADP, AMP, GTP, (p)ppGpp, uracil, and hypoxanthine) were performed using the HPLC (HITACHI, Japan) with a built-in diode-array detector (DAD) and a reversed-phase Gemini® 5 µm C18 110 Å column (Phenomenex) connected with a C-18 Supelguard™ Cartridge (4 mm × 3.0 mm; Phenomenex). The operating conditions were as follows: temperature 30°C, flow rate of 1 ml min^{-1} and DAD at absorbance 254 nm. The mobile phases consisted of two eluents: buffer A (20 mM ammonium acetate, pH 5.9, 4 mM tetrabutylammonium hydroxide, 0.1 mM NaN_3) and buffer B (40% buffer A and 60% acetonitrile). The following gradient was used: 15% buffer B for 12 min, 15%–40% buffer B for 36 min, 40%–100% buffer B for 15 min, 100% buffer B for 12 min, 100%–15% buffer B for 2 min, and then equilibration was done at 15% buffer B for 10 min to restore the initial conditions. After about 10 injections, the column was washed with 80% acetonitrile for 1 h. The injection volume was 40 µl for PCA extraction samples and 20 µl for cultivation supernatants. To avoid degradation of ATP and GTP, PCA extraction samples were analyzed immediately after removal from the −80°C freezer.

HPLC standards GTP and pppGpp were from Jena Bioscience GmbH. All other standards were purchased from Sigma-Aldrich.

2.5 | Other analytical procedures and calculations

Cell growth was monitored by measurement of the absorbance at 600 nm (OD_{600}). Biomass was determined using the standard curve of OD_{600} versus dry cell mass. One unit of OD_{600} corresponds to 0.39 g dry cell mass L^{-1} for *E. coli* BL21 (DE3). Off-gas analysis was performed in bioreactor cultures using the BlueInOne gas analyzer (BlueSens). The carbon dioxide and oxygen transfer rates were calculated as described previously (Kayser et al., 2005). The dissolved oxygen concentration was determined using a polarographic dissolved oxygen sensor (Mettler Toledo). For preparation of cell extracts and determination of soluble and insoluble product fractions, cells were disrupted by BugBuster™ Protein Extraction Reagent (Novagen) with Lysozyme and Benzonase according to the manufacturer's instructions. Soluble and insoluble cell fractions were separated by centrifugation at 17,000*g* and 4°C for 30 min. Sodium dodecyl sulfate-polyacrylamide gel electrophoresis (SDS-PAGE) analysis was performed in the Mini-Protean Tetra Cell (Bio-Rad) according to standard procedures and manufacturer's instructions. After electrophoresis, the proteins were visualized by colloidal Coomassie G-250 staining (Georgiou, Grintzalis, Zervoudakis, & Papapostolou, 2008). Quantification of target protein was done by densitometry from SDS-PAGE gels (GelAnalyzer; www.gelanalyzer.com).

3 | RESULTS

Reports on enhanced acetate formation and growth inhibition in response to recombinant protein production but also as a more general phenomenon observed during carbon overflow metabolism prompted us to compare the recombinant protein production-associated metabolic response with the response towards carbon overfeeding. For this purpose, cells were grown in a fed-batch procedure supporting a growth rate of $\mu_{set} = 0.35\ h^{-1}$. After reaching an optical density of $OD_{600} = 10$ (=3.9 g L^{-1} dry cell mass), the cells were either induced to produce the recombinant protein or exposed to carbon overfeeding by suddenly raising the exponential glucose feeding rate in such a way that it could support a growth rate of $\mu_{set} = 0.7\ h^{-1}$. The maximum growth rate of *E. coli* BL21 (DE3) is $\mu_{max} = 0.52\ h^{-1}$ during growth at 30°C using this medium, thus the carbon overfeeding conditions will certainly overwhelm the balanced carbon processing capacities of the cells. The initial situation before induction of protein production or before starting carbon overfeeding was in both types of experiments identical.

3.1 | Growth, glucose uptake, and primary metabolite formation (CO_2, acetate, pyruvate, and glutamate)

When cells are induced to produce hFGF-2 in fed-batch culture ($\mu_{set} = 0.35\ h^{-1}$) an obvious metabolic response became apparent approximately one and a half-hour after induction through a decline in the growth rate and the respiratory activity (Figure 1a). Before this decline, pyruvate started to accumulate in the culture medium followed by accumulation of acetate and glutamate (Figure 1b). Finally, accumulation of glucose was observed (Figure 1a). These data show that balanced glucose processing was impaired, most likely a result of limitations at the pyruvate node, leading to pyruvate and subsequently to acetate secretion. Glutamate secretion points to limitations in the TCA cycle from which the TCA cycle intermediate α-ketoglutarate can be transformed to glutamate under conditions of sufficient nitrogen supply and carbon excess. Interestingly, *E. coli* BL21 (DE3) appears to be able to counteract the reduced balanced glucose processing capacities by reducing the glucose uptake rate.

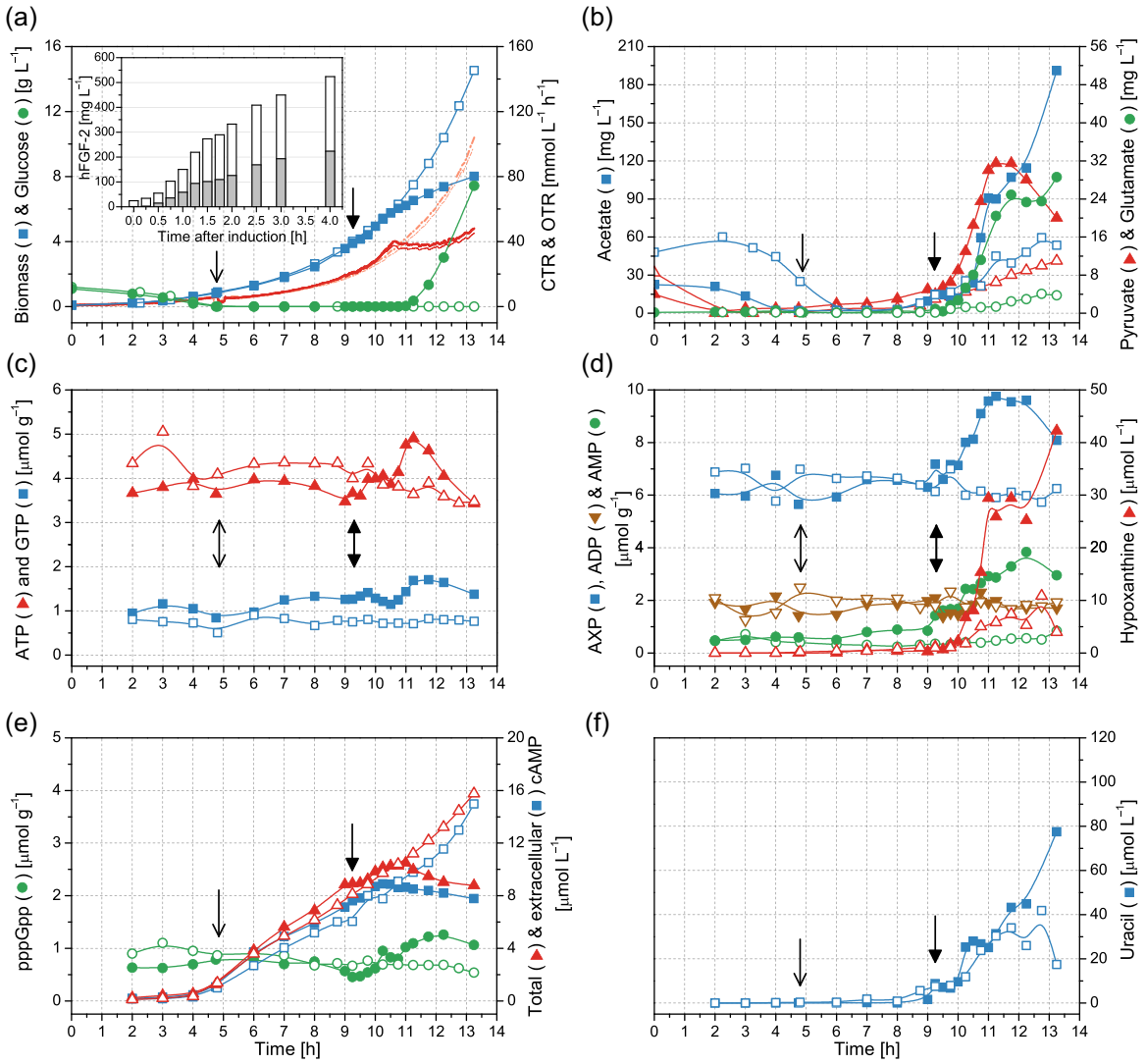

FIGURE 1 IPTG-induced production of hFGF-2 in fed-batch culture supporting growth at $\mu_{set} = 0.35\ h^{-1}$. (a) Time course of biomass (blue square) and glucose concentrations (green circle) and volumetric oxygen transfer rate (OTR, red thin line) and carbon dioxide transfer rates (CTRs, red thick line), (b) extracellular concentrations of acetate (blue square), pyruvate (red up-triangle) and glutamate (green circle), (c) intracellular concentrations of ATP (red up-triangle) and GTP (blue square), (d) intracellular concentrations of AMP (green circle), ADP (brown down-triangle) and AXP (blue square, sum of AMP, ADP, and ATP) and extracellular concentrations of hypoxanthine (red up-triangle), (e) intracellular concentrations of (p)ppGpp (green circle) and total (red up-triangle) and extracellular concentrations of cAMP (blue square) and (f) uracil (blue square). The inset in (a) shows the time-course of hFGF-2 production as concentration of soluble (white bar fraction) and insoluble (inclusion bodies) protein (gray bar fraction). Closed symbols and dark-colored lines always refer to the culture producing hFGF-2 and open symbols and light-colored lines to the control culture of *Escherichia coli* BL21 (DE3) without plasmid but with addition of IPTG. The thin and thick arrows, respectively, indicate the end of the batch phase and the time point of IPTG addition. cAMP, cyclic adenosine monophosphate; CTR, carbon dioxide transfer rate; hFGF-2, human basic fibroblast growth factor-2; IPTG, isopropyl β-D-1-thiogalactopyranoside [Color figure can be viewed at wileyonlinelibrary.com]

When cells were exposed to carbon overfeeding by increasing the exponential glucose feeding rate (not a glucose pulse!), cells instantaneously and strongly increased respiration for approximately 5 min followed by a period of almost constant respiratory activity of approximately 45 min, which was subsequently succeeded by a uniform but a more moderate exponential increase in the oxygen uptake and carbon dioxide formation rates (Figure 2a and inset therein). After initiation of carbon overfeeding, cell growth continued at the higher specific growth rate of $\mu = 0.45\ h^{-1}$ but considerably lower than the growth rate aimed for ($\mu_{set} = 0.7\ h^{-1}$) and also lower than the maximum growth rate possible ($\mu_{max} = 0.52\ h^{-1}$; Figure 2a, inset). After initiation of carbon overfeeding, accumulation of glucose, pyruvate, acetate, and glutamate occurred (Figure 2a,b). It was again notable that accumulation of pyruvate started before the accumulation of acetate. Again, accumulation of glucose demonstrates that *E. coli* BL21 (DE3) appears to be capable to control the glucose uptake, keeping the acetate concentration well below $1\ g\ L^{-1}$. However, the immediate response to the higher glucose availability was a

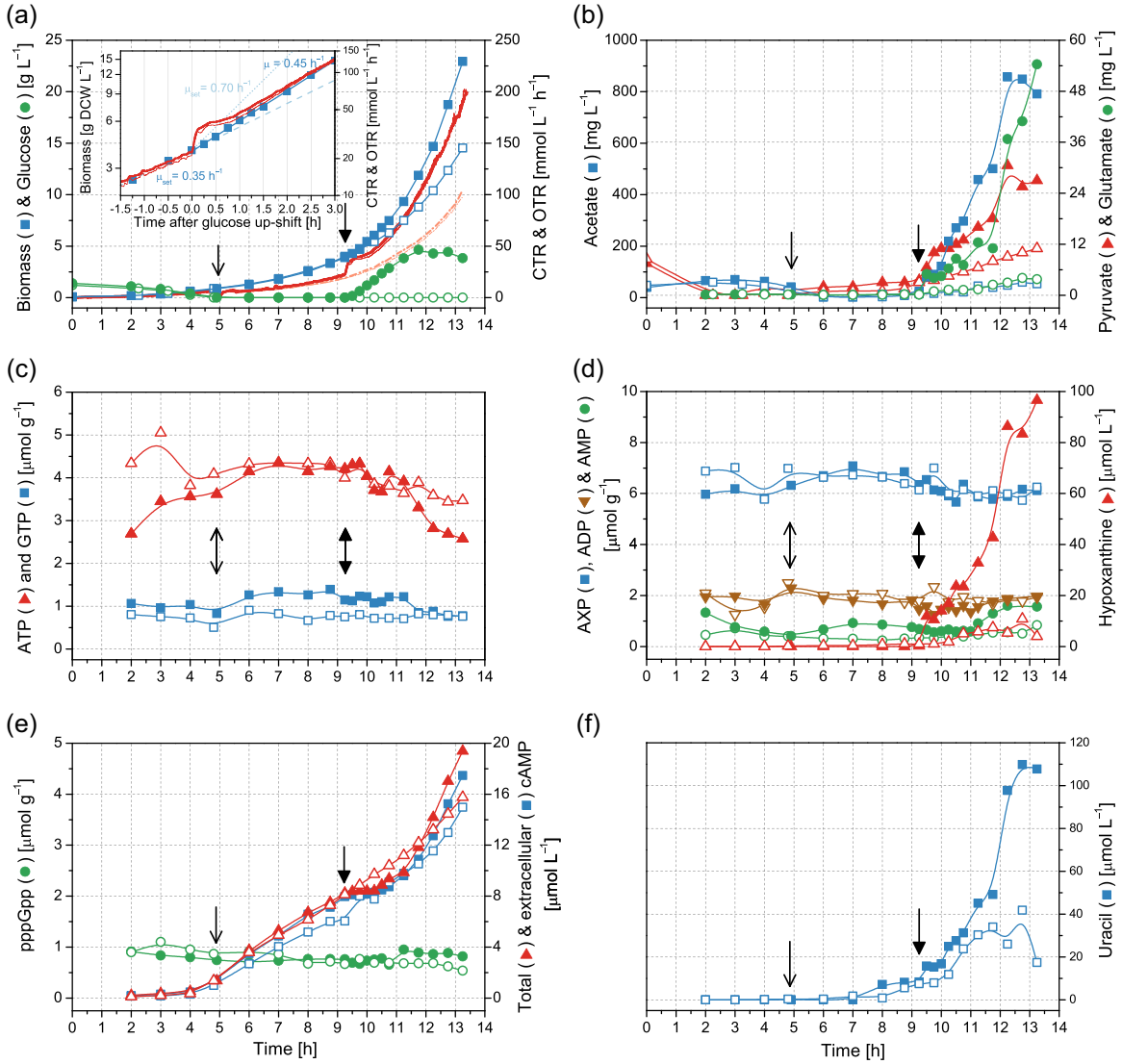

FIGURE 2 Carbon overfeeding of *Escherichia coli* BL21 (DE3) growing at μ_{set} = 0.35 h^{-1} through changing to fed-batch conditions supporting growth at μ_{set} = 0.7 h^{-1}. (a) Time course of biomass (blue square) and glucose concentrations (green circle) and volumetric oxygen transfer rate (OTR, red thin line) and carbon dioxide transfer rates (CTRs, red thick line), (b) extracellular concentrations of acetate (blue square), pyruvate (red up-triangle) and glutamate (green circle), (c) intracellular concentrations of ATP (red up-triangle) and GTP (blue square), (d) intracellular concentrations of AMP (green circle), ADP (brown down-triangle) and AXP (blue square, sum of AMP, ADP, and ATP) and extracellular concentrations of hypoxanthine (red up-triangle), (e) intracellular concentrations of (p)ppGpp (green circle) and total (red up-triangle) and extracellular concentrations of cAMP (blue square) and (f) uracil (blue square). The inset in (a) shows the real growth rate (blue solid line), respectively, biomass concentration (blue square), after initiation of carbon overfeeding in comparison to the original growth rate of μ_{set} = 0.35 h^{-1} (light blue broken line) and the intended growth rate of μ_{set} = 0.7 h^{-1} (light blue dotted line). Moreover, the inset also depicts the time course of volumetric oxygen uptake (red thin line) and carbon dioxide formation rates (red thick line). Please note that biomass and respiratory rates are depicted in the inset in half logarithmic scale. Closed symbols and dark-colored lines always refer to the culture subjected to carbon overfeeding and open symbols and light-colored lines to the control culture continuing growth at conditions supporting the growth rate of μ_{set} = 0.35 h^{-1} (control culture as in Figure 1). The thin and thick arrows, respectively, indicate the end of the batch phase and the time point of initiation of carbon overfeeding. cAMP, cyclic adenosine monophosphate; CTR, carbon dioxide transfer rate; hFGF-2, human basic fibroblast growth factor-2; IPTG, isopropyl β-D-1-thiogalactopyranoside [Color figure can be viewed at wileyonlinelibrary.com]

sudden strong increase in catabolic (respiratory) activity, indicating that respiration presumably does not limit balanced cell growth.

Similarities in the response towards recombinant protein production or carbon overfeeding include resulting limitations at the pyruvate node and TCA cycle as well as an adaptive reduction in the glucose uptake rate. The response towards induced protein production, however, occurs with a delay (approximately one and a half hours at the employed conditions) and reflects a persistent perturbation. The response towards carbon overfeeding, on the other hand, occurs instantaneously, involving initially enhanced respiration rates (approximately 5 min) followed by an adaptation period with reduced rates of approximately 1 h until cells continue to

respire and grow in a seemingly balanced state although at rates lower than possible.

3.2 | Energy-rich compounds (ATP and GTP)

ATP and GTP are not only precursors for RNA synthesis but also serve as energy currency with ATP as the most important compound for energy exchange. As protein synthesis is an energy-costly process, the analysis of these compounds will give valuable hints if energy limitation could be a major factor of the protein production-associated metabolic burden.

The analysis of the intracellular ATP content did not reveal any decrease for the first two hours after induction of hFGF-2 synthesis (Figure 1c). In contrast, there was a transient increase in ATP, and decreasing ATP levels were first observed after the decline of the respiratory activity. As the majority of hFGF-2 is produced during the first two hours (see Figure 1a, inset), energetic restrictions are unlikely to contribute to the recombinant protein production-associated metabolic burden. These data also indicate that the later observed ATP decline is the result but not the reason the recombinant protein production-associated metabolic perturbations. The time-course data of GTP revealed a similar trend, confirming the above conclusions.

The time-course data of the energy-rich compounds ATP and GTP after exposure to carbon overfeeding did not reveal any obvious short-term increase but a more general decline after initiation of overfeeding conditions (Figure 2c). This decline was more obvious for ATP than for GTP. However, it should be noted that no samples were taken for ATP and GTP analysis during the first initial burst phase of respiratory activity (5 min) after initiation of carbon overfeeding.

3.3 | Degradation products of purine metabolism (ADP, AMP, hypoxanthine)

The initial degradation products of ATP are the lower energy-containing nucleotides ADP and AMP. Further degradation leads to the nucleobase adenine, which is further degraded to hypoxanthine (Leung & Schramm, 1980). Hypoxanthine formation is not only observed in bacteria but also in other organisms including humans, where it is considered as a general stress indicator (Mellon et al., 2019; Pechlivanis et al., 2015).

Interestingly, the sum of all AXP increased in response to hFGF-2 production, pointing to de novo synthesis of AXP nucleotides and not only to regenerative ATP turnover from ADP/AMP (Figure 1d). Moreover, accumulation of hypoxanthine occurred in response to recombinant protein synthesis, suggesting enhanced degradation of AXP nucleotides (Figure 1d). ATP did not decrease at the onset of hypoxanthine secretion, in contrast, ATP still increased when hypoxanthine started to accumulate in the culture medium (Figure 1c,d), indicating that hampered ATP utilization may induce AXP degradation pathways.

In the culture exposed to carbon overfeeding the sum of all AXP nucleotides did not increase, however, hypoxanthine secretion was immediately observed after the initiation of carbon overfeeding, presumably also indicating insufficient demand for adenosine nucleotides (Figure 1d). Altogether, these findings suggest that ATP homeostasis is particularly hampered in cells induced to produce recombinant proteins but also in cells exposed to carbon overfeeding.

3.4 | Regulatory molecules (cAMP and (p)ppGpp)

Induced recombinant protein production but also carbon overfeeding has an impact on glucose metabolism. Thus, it is of interest to follow the concentration of the most important regulatory molecule of carbon metabolism, cyclic AMP (cAMP). cAMP increases instantaneously when cells encounter glucose starvation, for example, during entry into a stationary phase, with the majority being excreted into the medium (Buettner, Spitz, & Rickenberg, 1973; Makman & Sutherland, 1965). Moreover, (p)ppGpp, nutrient stress but also more general stress-sensing molecule (Dalebroux & Swanson, 2012), was followed after induced synthesis of hFGF-2 or carbon overfeeding.

At the end of the batch phase and during the fed-batch phase, extracellular cAMP concentrations gradually increased (Figures 1e and 2e). When production of hFGF-2 was induced, cAMP concentrations continued to increase for approx. one and a half-hour more and then slowly declined afterwards (Figure 1e). When cells were exposed to carbon overfeeding, extracellular cAMP concentrations immediately stopped increasing for about one hour and subsequently resumed to increase at a higher rate (Figure 2e). Analysis of the cellular (p)ppGpp content revealed an increase after induction of hFGF-2 synthesis (Figure 1e) but no significant change in the culture that was exposed to carbon overfeeding (Figure 2e).

3.5 | RNA degradation (extracellular accumulation of uracil)

When cells reach the stationary phase or encounter growth perturbing conditions (ribosomal) RNA degradation occurs followed by extracellular uracil accumulation (Rinas, Hellmuth, Kang, Seeger, & Schlieker, 1995).

Analysis of the culture medium revealed that extracellular uracil concentrations increased during the production of hFGF-2 in the fed-batch culture (Figure 1f). However, extracellular uracil concentrations also increased in the fed-batch phase of the nonproducing control culture although less pronounced. In the culture exposed to carbon overfeeding uracil accumulated even more rapidly (Figure 2f).

These data indicate that the growth inhibitory effect of recombinant protein production or carbon overfeeding leads to degradation of RNA and thus also indicates that there are presumably no limitations to the availability of RNA precursor metabolites.

3.6 | What happens when carbon feeding is reduced during hFGF-2 production?

Usually production of hFGF-2 but also of other proteins is carried out at lower feeding rates in fed-batch cultures to circumvent the problem of growth inhibition and acetate formation (Hoffmann et al., 2004). To analyze the cellular response towards production of hFGF-2 at reduced carbon feeding, cells were grown in a fed-batch procedure supporting a growth rate of $\mu_{set} = 0.12\ h^{-1}$ (instead of $\mu_{set} = 0.35\ h^{-1}$).

The analyses revealed a neglectable growth inhibition in the hFGF-2 producing culture compared to the induced control culture not carrying any plasmid (Figure 3a). Glucose accumulation was not observed. Moreover, hFGF-2 was produced at a lower rate and almost exclusively as a soluble protein (see inset in Figure 3a). Acetate excretion was marginal and comparable to the control culture, accumulation of pyruvate was not observed (Figure 3b). However, the ATP also increased during production of hFGF-2 at conditions of slow carbon feeding (Figure 3b). Simultaneous to the ATP increase, accumulation of hypoxanthine occurred (Figure 3c), (p)ppGpp increased, and the extracellular accumulation of cAMP ceased (Figure 3d). These data show that the basic cause for the metabolic burden is still present at slow carbon feeding, but the cells are able to better balance catabolic and anabolic metabolism.

3.7 | Is the phenomenon unique to the production of hFGF-2?

Production of hFGF-2 leads to a strong growth inhibition when production was carried out in fed-batch cultures using a feeding protocol that supports growth at $\mu_{set} = 0.35\ h^{-1}$. Thus, it was tested if the production of other proteins using the T7-based expression system and the described fed-batch conditions were causing similar responses.

Production of GFP and GST-GFP also caused growth inhibition but less severe compared to the inhibition resulting from hFGF-2 production (Figure 4a). In addition, glucose accumulated in all producing cultures, the more severe the growth inhibition, the earlier

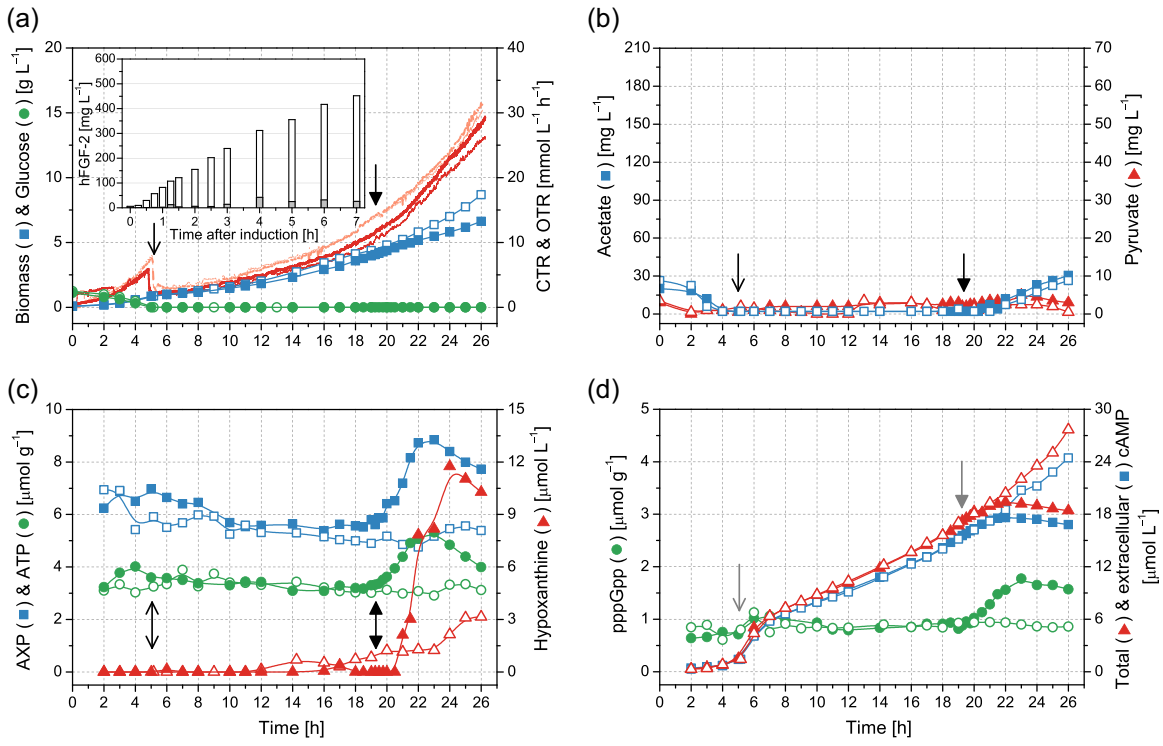

FIGURE 3 IPTG-induced production of hFGF-2 in fed-batch culture supporting growth at $\mu_{set} = 0.12\ h^{-1}$. (a) Time course of biomass (blue square) and glucose concentrations (green circle), volumetric oxygen transfer rate (OTR, red thick line) and carbon dioxide transfer rates (CTRs, red thin line), and (b) extracellular concentrations of acetate (blue square) and pyruvate (red up-triangle) (c) intracellular concentrations of ATP (green circle) and AXP (blue square, sum of AMB, ADP, and ATP) and extracellular concentrations of hypoxanthine (red up-triangle), (d) intracellular concentrations of (p)ppGpp (green circle) and total (red up-triangle) and extracellular concentrations of cAMP (blue square). The inset in (a) shows the time-course of hFGF-2 production as concentration of soluble (white bar fraction) and insoluble (inclusion bodies) protein (gray bar fraction). Closed symbols and dark-colored lines always refer to the culture producing hFGF-2 and open symbols and light-colored lines to the control culture of *Escherichia coli* BL21 (DE3) without plasmid but with the addition of IPTG. The thin and thick arrows, respectively, indicate the end of the batch phase and the time point of IPTG addition. cAMP, cyclic adenosine monophosphate; hFGF-2, human basic fibroblast growth factor-2; IPTG, isopropyl β-D-1-thiogalactopyranoside; (p)ppGpp, guanosine pentaphosphate [Color figure can be viewed at wileyonlinelibrary.com]

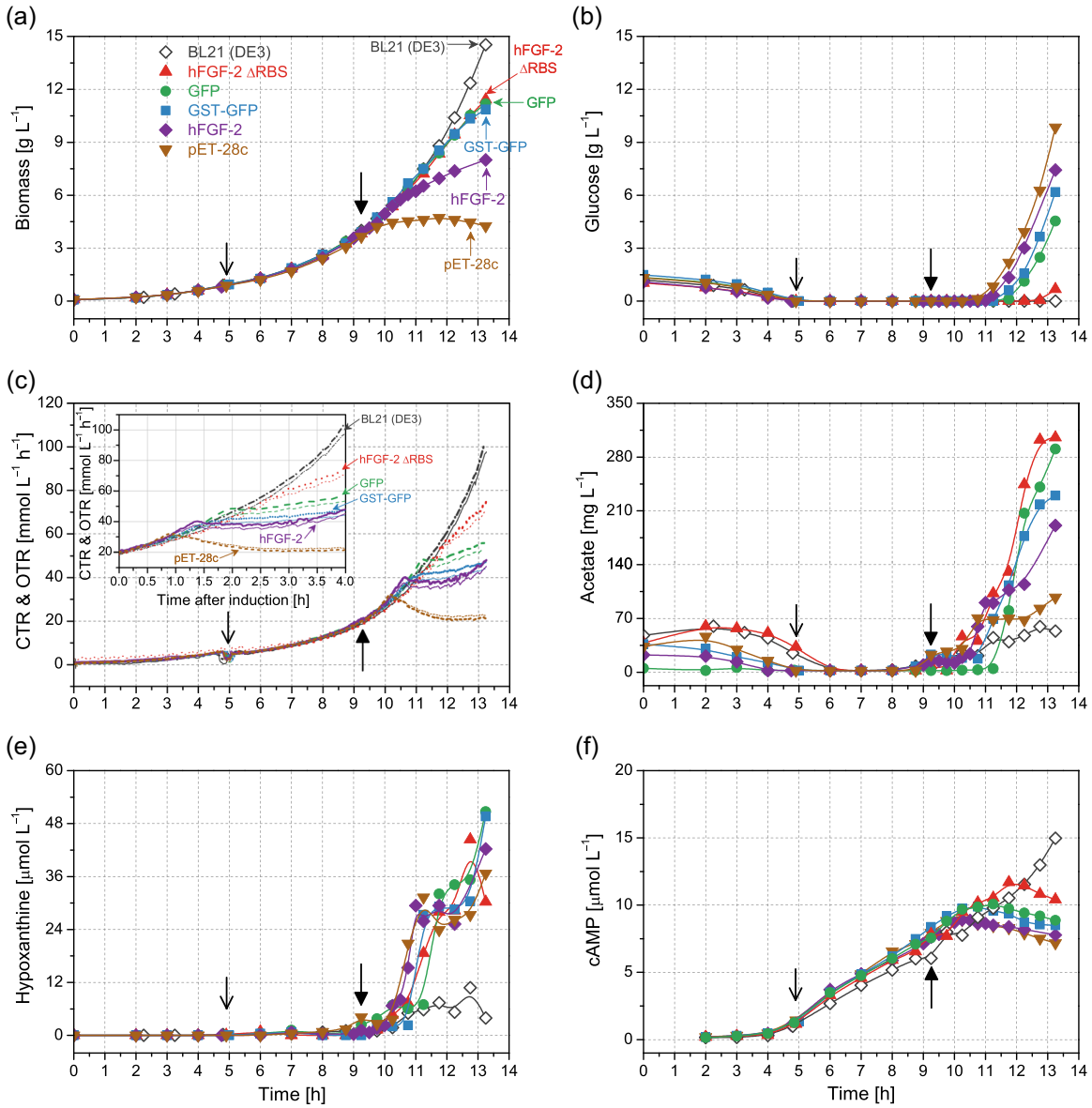

FIGURE 4 IPTG-induction of *Escherichia coli* BL21 (DE3) carrying different T7 promoter controlled plasmids in fed-batch culture supporting growth at $\mu_{set} = 0.35\ h^{-1}$. Time course of (a) biomass, (b) glucose concentrations, (c) volumetric oxygen transfer rate (OTR, thin line) and carbon dioxide transfer rates (CTRs, thick line), (d) extracellular concentrations of acetate, (e) hypoxanthine, and (f) cAMP. *E. coli* BL21 (DE3) producing hFGF-2 (purple diamonds and purple solid lines), GST-GFP (blue squares and blue dotted lines) and GFP (green circles and green broken lines), and *E. coli* BL21 (DE3) carrying the expression vector without ribosome binding sites allowing only transcription of the hFGF-2 gene but no translation into protein (red up-triangles and red short broken lines). *E. coli* BL21 (DE3) carrying the expression vector pET-28c without inset (brown down-triangles and brown short broken lines) and control culture of *E. coli* BL21 (DE3) without plasmid but with addition of IPTG (black open diamonds and black broken lines with dots). The thin and thick arrows, respectively, indicate the end of the batch phase and the time point of IPTG addition. cAMP, cyclic adenosine monophosphate; GFP, green fluorescent protein; GST, glutathione S-transferase; hFGF-2, human basic fibroblast growth factor-2; IPTG, isopropyl β-D-1-thiogalactopyranoside [Color figure can be viewed at wileyonlinelibrary.com]

the onset of glucose accumulation (Figure 4b), and the decline in the respiratory activity (Figure 4c). Hypoxanthine also accumulated in all producing cultures (Figure 4e), again, the more severe the growth inhibition, the earlier the onset of hypoxanthine accumulation. In all producing cultures, cAMP accumulation ceased shortly before glucose started to accumulate (Figure 4f).

Finally, it was tested if the expression of the recombinant gene without translation into the protein product caused similar metabolic perturbations. Induced transcription of the hFGF-2 gene without hFGF-2 synthesis (deletion of ribosome binding sites, (Li & Rinas, 2020) was also leading to growth inhibition, connected to glucose and hypoxanthine accumulation and cessation of cAMP accumulation (Figure 4). Moreover, also IPTG induction of cells transformed with the "empty" expression vector pET-28c without the inserted gene but still transcribing a 225 bp fragment caused strong growth inhibition with the above similarities in glucose and

hypoxanthine accumulation and cessation of cAMP accumulation (Figure 4).

4 | DISCUSSION

A comparison of the protein production-associated metabolic burden and the response towards carbon overfeeding revealed similarities, which point to limitations in anabolic and not in catabolic pathways. Our data also show clearly that cells do not experience energy limitations during the protein production period. In contrast, accumulation of ATP and other energy-rich metabolites such as GTP are observed and the excess of adenine nucleotides is subjected to degradation pathways. Also, our data do not indicate a shortage in RNA precursor nucleotides. In contrast, we see an increase in RNA breakdown products (e.g., uracil). In addition, accumulation of pyruvate—an important amino acid precursor—as well as glutamate indicates that there are no shortages of amino acids and their precursors. In particular, the accumulation of glutamate, a successor molecule of the TCA-cycle intermediate α-ketoglutarate, indicates insufficient precursor withdrawal from the TCA cycle for anabolic functions. Our data are consistent with the assumption that limitations in anabolic pathways are restricting growth. These restrictions are not a result of enhanced drainage of energy and precursor molecules for nucleotides and amino acids away from host cells towards plasmid-encoded functions. Most likely, the recombinant gene transcription and recombinant protein production-related growth inhibition is caused through interference with more complex anabolic processes.

It has been proposed that respiratory energy generation might be a growth-limiting bottleneck (Anderson & von Meyenburg, 1980) and more recently, the high energetic costs for synthesizing the enzymatic inventory for respiratory energy generation have been held responsible for restricting growth, leading to carbon overflow metabolism with the well-known consequences of acetate formation and resultant growth inhibition (Basan et al., 2015; Zeng & Yang, 2019a). Our data do not indicate restrictions in respiratory energy generation. In contrast, respiratory activity soars instantaneously for a short period (approximately 5 min) in response to carbon overfeeding followed by an adaptation period until a new (pseudo) steady state is reached (Figure 2a). In the hFGF-2 producing culture, ATP levels still increase after the decline in respiratory activity until they finally start to decrease (Figure 1). Altogether, these data do not show limitations in respiratory ATP generation but suggest that cells which are not able to utilize the generated ATP reduce respiratory activity trying to keep a balanced energetic status within the cell.

The delayed arrest of cAMP accumulation upon induction signals that the recombinant cells are running into a metabolic status of too much carbon inflow, which cannot be processed adequately in anabolic pathways. In the culture exposed to carbon overfeeding, cAMP accumulation immediately stops after increasing the glucose feed signaling carbon excess conditions. In the protein-producing culture as well as in the culture exposed to carbon overfeeding, cessation of cAMP accumulation in the culture broth coincides with the onset of glucose accumulation in the culture medium (Figures 1 and 2). Excessive acetate formation, usually observed in *E. coli* K strains (Shiloach & Rinas, 2009; Shiloach et al., 1996), does not occur presumably because *E. coli* BL21 is capable of better adjusting glucose uptake to anabolic consumption. In the culture exposed to carbon overfeeding, cAMP accumulation resumes one hour after initiation of carbon overfeeding, (Figure 2) but in the hFGF-2 producing culture as well as in the other induced recombinant cultures, arrest of cAMP accumulation is observed for the remainder of the cultivation indicating ongoing sensing of carbon overflow conditions (Figures 1 and 4). Thus, the characteristic pattern of extracellular cAMP concentrations in fed-batch cultures can be used as a reliable reporter of fitness of protein-producing cells (see also Lin et al., 2004) signaling their reduced capacities for balanced carbon processing.

In addition, detection of increasing extracellular hypoxanthine concentrations can be used as an indicator of activation of adenine nucleotide degradation pathways initially as a result of insufficient ATP consumption. Accumulation of uracil also points to stressful conditions but extracellular uracil also increases during regular entry into the stationary phase when ribosome degradation occurs (Rinas et al., 1995) and may only serve as an additional indicator of stress during recombinant protein production. Accumulation of (p)ppGpp, as a general stress indicator, can also signal stress conditions during recombinant protein production, however there are conflicting results on (p)ppGpp levels as an informative reporter on the fitness of protein-producing cells (Lin et al., 2004).

Growth inhibition is often enhanced when cells are producing under conditions supporting rapid growth. When production of hFGF-2 is carried out at slow carbon feeding conditions, growth inhibition is neglectable and accumulation of glucose is not observed (Figure 3). However, production of hFGF-2 at slow carbon feeding also leads to ATP accumulation and hypoxanthine secretion as well as to cessation of cAMP accumulation. Thus, cells still appear to sense these conditions as "carbon excess conditions" however, at this reduced carbon inflow, the anabolic capacities of the cells do not appear to be overloaded.

The metabolic response is also not unique to the production of hFGF-2 but also observed during the production of other proteins. It even occurs during induction of recombinant gene transcription without recombinant protein synthesis and can also occur when short transcripts are made from "empty" expression vectors. The onset and extent of the metabolic response, however, depends on the specific expression system: the more severe the growth inhibition, the earlier the onset of hypoxanthine accumulation, cessation of cAMP accumulation, and start of glucose accumulation.

5 | CONCLUSIONS

In conclusion, the growth inhibitory metabolic response towards recombinant protein production is delayed, persistent, and based on constraints in anabolic pathways. Contrary to expectations, neither energy generation nor provision of precursor metabolites for

nucleotides and amino acids limits host cell and plasmid-encoded functions. In contrast, accumulation of catabolic by-products, for example, pyruvate, acetate, and glutamate and energy spillage, for example, accumulation and degradation of adenine nucleotides with concomitant accumulation of extracellular hypoxanthine reflect overwhelming carbon catabolism and insufficient anabolic utilization. The cellular response towards insufficient anabolic carbon utilization involves downregulation of cAMP formation, presumably responsible for subsequently better-controlled glucose uptake and the resultant accumulation of glucose in the culture medium. Growth inhibition is neglectable when protein production is induced at conditions supporting slower growth through reduced carbon availability. At these conditions, the reduced carbon supply does not overburden the compromised anabolic capacities of producing cells. The growth inhibitory effect with accompanying energy spillage, respectively, hypoxanthine secretion and cessation of cAMP formation is observed in response to the production of various proteins but also during overexpression of genes without transcript translation, and even when short transcripts are formed from "empty" expression vectors.

ACKNOWLEDGMENTS

Partial financial support was received from the German Ministry of Education and Research (BMBF) through the FORSYS-Partner program (grant FKZ 0315285) and from the German Research Council (DFG) through the Cluster of Excellence "Rebirth" EXC62. Open access funding enabled and organized by Projekt DEAL.

CONFLICT OF INTERESTS

The authors declare that there are no conflict of interests.

AUTHOR CONTRIBUTIONS

Zhaopeng Li carried out the experiments and performed the data analysis and prepared a first draft of the manuscript. Ursula Rinas directed the study and prepared the final manuscript. All authors read and approved the final manuscript.

ORCID

Ursula Rinas http://orcid.org/0000-0003-4940-5749

REFERENCES

Anderson, K. B., & von Meyenburg, K. (1980). Are growth rates of *Escherichia coli* in batch cultures limited by respiration? *Journal of Bacteriology*, *144*, 114–123.

Basan, M., Hui, S., Okano, H., Zhang, Z., Shen, Y., Williamson, J. R., & Hwa, T. (2015). Overflow metabolism in *Escherichia coli* results from efficient proteome allocation. *Nature*, *528*, 99–104.

Buettner, M. J., Spitz, E., & Rickenberg, H. V. (1973). Cyclic adenosine 3', 5'-monophosphate in *Escherichia coli*. *Journal of Bacteriology*, *114*, 1068–1073.

Corrales, F. J., & Fersht, A. R. (1996). Toward a mechanism for GroEL·GroES chaperone activity: An ATPase-gated and -pulsed folding and annealing cage. *Proceedings of the National Academy of Sciences of the United States of America*, *93*, 4509–4512.

Cserjan-Puschmann, M., Kramer, W., Duerrschmid, E., Striedner, G., & Bayer, K. (1999). Metabolic approaches for the optimisation of recombinant fermentation processes. *Applied Microbiology and Biotechnology*, *53*, 43–50.

Dalebroux, Z. D., & Swanson, M. S. (2012). ppGpp: Magic beyond RNA polymerase. *Nature Reviews Microbiology*, *10*, 203–212.

Georgiou, C. D., Grintzalis, K., Zervoudakis, G., & Papapostolou, I. (2008). Mechanism of coomassie brilliant blue G-250 binding to proteins: A hydrophobic assay for nanogram quantities of proteins. *Analytical and Bioanalytical Chemistry*, *391*, 391–403.

Hoffmann, F., van den Heuvel, J., Zidek, N., & Rinas, U. (2004). Minimizing inclusion body formation during recombinant protein production in *Escherichia coli* at bench and pilot plant scale. *Enzyme and Microbial Technology*, *34*, 235–241.

Kaleta, C., Schäuble, S., Rinas, U., & Schuster, S. (2013). Metabolic costs of amino acid and protein production in *Escherichia coli*. *Biotechnology Journal*, *8*, 1105–1114.

Korz, D. J., Rinas, U., Hellmuth, K., Sanders, E. A., & Deckwer, W. D. (1995). Simple fed-batch technique for high cell density cultivation of *Escherichia coli*. *Journal of Biotechnology*, *39*, 59–65.

Leung, H. B., & Schramm, V. L. (1980). Adenylate degradation in *Escherichia coli*. *Journal of Biological Chemistry*, *255*, 10867–10874.

Li, Z., Kessler, W., van den Heuvel, J., & Rinas, U. (2011). Simple defined autoinduction medium for high-level recombinant protein production for T7-based *Escherichia coli* expression systems. *Applied Microbiology and Biotechnology*, *91*, 1203–1213.

Li, Z., Nimtz, M., & Rinas, U. (2014). The metabolic potential of *Escherichia coli* BL21 in defined and rich medium. *Microbial Cell Factories*, *13*, 45.

Li, Z., & Rinas, U. (2020). Recombinant protein production associated growth inhibition results mainly from transcription and not from translation. *Microbial Cell Factories*, *19*, 83.

Lin, H., Hoffmann, F., Rozkov, A., Enfors, S.-O., Rinas, U., & Neubauer, P. (2004). Change of extracellular cAMP concentration is a sensitive reporter for bacterial fitness in high-cell-density cultures of *Escherichia coli*. *Biotechnology and Bioengineering*, *87*, 602–613.

Makman, R. S., & Sutherland, E. W. (1965). Adenosine 3', 5'-phosphate in *Escherichia coli*. *Journal of Biological Chemistry*, *240*, 1309–1314.

Mellon, S. H., Bersani, F. S., Lindqvist, D., Hammamieh, R., Donohue, D., Dean, K., … Wolkowitz, O. M. (2019). Metabolomic analysis of male combat veterans with post traumatic stress disorder. *PLOS One*, *14*, e0213839.

Mittal, P., Brindle, J., Stephen, J., Plotkin, J. B., & Kudla, G. (2018). Codon usage influences fitness through RNA toxicity. *Proceedings of the National Academy of Sciences of the United States of America*, *115*, 8639–8644.

Mori, M., Marinari, E., & De, M. A. (2019). A yield-cost tradeoff governs *Escherichia coli*'s decision between fermentation and respiration in carbon-limited growth. *NPJ Systems Biology and Applications*, *5*, 16.

Pechlivanis, A., Papaioannou, K. G., Tsalis, G., Saraslanidis, P., Mougios, V., & Theodoridis, G. A. (2015). Monitoring the response of the human urinary metabolome to brief maximal exercise by a combination of RP-UPLC-MS and (1)H NMR spectroscopy. *Journal of Proteome Research*, *14*, 4610–4622.

Rinas, U., Hellmuth, K., Kang, R., Seeger, A., & Schlieker, H. (1995). Entry of *Escherichia coli* into stationary phase is indicated by endogenous and exogenous accumulation of nucleobases. *Applied and Environmental Microbiology*, *61*, 4147–4151.

Sharma, S. K., De los, R. P., Christen, P., Lustig, A., & Goloubinoff, P. (2010). The kinetic parameters and energy cost of the Hsp70 chaperone as a polypeptide unfoldase. *Nature Chemical Biology*, *6*, 914–920.

Shiloach, J., Kaufmann, J., Guillard, A. S., & Fass, R. (1996). Effect of glucose supply strategy on acetate accumulation, growth, and recombinant protein production by *Escherichia coli* BL21 (λDE3) and *Escherichia coli* JM109. *Biotechnology and Bioengineering*, *49*, 421–428.

Shiloach, J., & Rinas, U. (2009). Glucose and acetate metabolism in *E. coli* - System level analysis and biotechnological applications in protein

production processes. In S. Y. Lee (Ed.), *Systems biology and biotechnology of* Escherichia coli (pp. 377–400). Berlin, Heidelberg, New York: Springer-Verlag.

Stouthamer, A. H. (1973). A theoretical study on the amount of ATP required for synthesis of microbial cell material. *Antonie Van Leeuwenhoek*, *39*, 545–565.

Studier, F. W., & Moffatt, B. A. (1986). Use of bacteriophage T7 RNA polymerase to direct selective high-level expression of cloned genes. *Journal of Molecular Biology*, *189*, 113–130.

Szabo, A., Langer, T., Schröder, H., Flanagan, J., Bukau, B., & Hartl, F. U. (1994). The ATP hydrolysis-dependent reaction cycle of the *Escherichia coli* Hsp70 system—DnaK, DnaJ, and GrpE. *Proceedings of the National Academy of Sciences of the United States of America*, *91*, 10345–10349.

Zeng, H., & Yang, A. (2019a). Modelling overflow metabolism in *Escherichia coli* with flux balance analysis incorporating differential proteomic efficiencies of energy pathways. *BMC Systems Biology*, *13*, 3.

Zeng, H., & Yang, A. (2019b). Quantification of proteomic and metabolic burdens predicts growth retardation and overflow metabolism in recombinant *Escherichia coli*. *Biotechnology and Bioengineering*, *116*, 1484–1495.

How to cite this article: Li Z, Rinas U. Recombinant protein production-associated metabolic burden reflects anabolic constraints and reveals similarities to a carbon overfeeding response. *Biotechnology and Bioengineering*. 2021;118:94–105. https://doi.org/10.1002/bit.27553